Int J Adv Manuf Technol (2018) 94:867–880
DOI 10.1007/s00170-017-0971-0

ORIGINAL ARTICLE

An investigation on flaring process of thin-walled tubes using multistage single point incremental forming

Hamed Movahedinia[1] · **Mohammad Javad Mirnia**[1] · **Majid Elyasi**[1] · **Hamid Baseri**[1]

Received: 15 February 2017 / Accepted: 14 August 2017 / Published online: 21 August 2017

Abstract The flaring of a thin-walled tube is conventionally carried out by pressing the tube end using dedicated die sets. As an alternative process with the high flexibility and low complexity, in this research, the utilization of single point incremental forming (SPIF), which is the simplest variant of incremental sheet metal forming (ISMF) processes, was assessed and investigated experimentally and numerically for flaring of the tube end. Results predicted by the finite element (FE) model through the commercial code Abaqus/Explicit showed a reasonable agreement with the experimental results. In the present research, the formability in SPIF was compared with that in pressing process and it was concluded that using multistage SPIF, the maximum semi-cone angle achievable before fracture can be improved at least 100%. The results showed that the thickness distribution in the conical flaring of the tube end includes thinning and thickening regions affected by the deformation strategy of multistage SPIF. In this regard, the formability of the tube end and the material deformation were studied under various forming strategies. Finally, for non-axisymmetric flaring of the tube end in the form of a pyramid with the semi-angle of 20° using SPIF, different three-stage forming strategies were designed and successfully implemented. The thickness distribution and the geometric accuracy under designed three-stage strategies were investigated.

✉ Mohammad Javad Mirnia
mirnia@nit.ac.ir

[1] Mechanical Engineering Department, Babol Noshirvani University of Technology, Babol 4714871167, Iran

Keywords Tube flaring · Single point incremental forming (SPIF) · Multistage forming · Thickness distribution · Formability

1 Introduction

The forming process of thin-walled tubes has wide applications in aerospace, automotive, and ship building industries. One of the most concerned processes in this field is the forming of tubes end through nosing or flaring processes. The tube end flaring is often carried out in the form of axisymmetric geometries using a dedicated die and punch. In this process, a conical punch with a specified semi-angle is pressed into the free end of the tube by a desired ram displacement.

Several works have focused on the tube end flaring to predict the success of the process and avoid possible defects like the edge crack, the wall wrinkling, and the local buckling. Huang [1] numerically studied the aluminum tube end flaring using conical punches with different semi-angles at various ram displacements. The results showed that at the semi-cone angle of 52°, the edge curling can occur. Therefore, this angle was considered as a critical angle. Lu [2] performed experimental and theoretical investigations on the formability of the stainless steel in the tube end flaring at the angles of 20°, 30°, and 45° with considering different friction conditions. It was concluded that the maximum expansion ratio and forming depth can be achieved at the semi-cone angles of 45° and 20°, respectively. Theoretical and experimental studies of the forming of thin-walled AA6060 tubes by Almeida et al. [3] showed that the formability in the flaring and nosing process can be limited by the ductile fracture, local buckling, and wrinkling which are significantly affected by the friction. The flaring and nosing processes of two-layer metal tubes were considered by Huang [4], and it was recommended to

locate the tube with the higher strength on the outer side and the one with the lower strength on the inner side for obtaining better results. The elliptical flaring of titanium microtubes using a two-stage forming strategy was investigated by Nikhare et al. [5]. They evaluated the effect of the geometry of the first punch on the strain path and the tube expansion using the numerical simulation. The maximum expansion ratio was obtained by implementing a circular punch at the first stage. To reach a uniform thickness distribution and mechanical properties, Zhao et al. [6] carried out the tube spinning together with the tube end flaring as a hybrid process on titanium tubes. In their research, firstly, a preform with a variable thickness distribution was produced using the spinning process and then it was formed to the final shape by the tube flaring process at high temperatures.

The utilization of dedicated die and punch sets, especially in the multistage forming with high tooling costs, can only be economically reasonable for the mass production. On the other hand, for the customized production, processes with the high flexibility and low-cost tooling such as the incremental sheet metal forming (ISMF) can be promising. Some initial variants of ISMF were proposed by Roux in 1960 and Leszak in 1967 as US patents [7]. With development of more advanced computer numerically controlled (CNC) machines, ISMF has attained much attention from academic researchers. The simplest variant of ISMF is single point incremental forming (SPIF). In SPIF, a hemispherical rigid tool controlled by a CNC movement gradually and locally deforms a sheet metal along a predetermined path generated based on the desired geometry of the final part. Owing to its high flexibility and low-cost tooling, SPIF can be considered as a rapid prototyping process for sheet metal parts.

Several researches have dealt with SPIF. Shim and Park [8] experimentally compared the formability of an annealed AA1050 aluminum sheet in conventional forming processes with that in SPIF and showed that the higher formability can be reached using SPIF. Hussain and Gao [9] proposed a new fast formability test based on a variable wall angle cone to predict the limiting wall angle during SPIF. Jackson and Allwood [10] experimentally compared the deformation mechanics of copper sheets in SPIF and two point incremental forming (TPIF) with that in a conventional stamping process. They concluded that the existence of shear strain parallel and perpendicular to the tool movement direction is the main difference between ISMF and stamping process. To assess the formability of AA6082-T6 sheet metal in SPIF of a truncated cone, Manco and Ambrogio [11] conducted a design of experiment (DOE) through which the effect of the process parameters including the tool diameter, the vertical pitch, the initial thickness, and the wall angle was investigated. The results revealed that the minimum thickness is not significantly affected by the tool diameter and increases with increasing the vertical pitch. Hamilton and Jeswiet [12] analyzed the effect of the rotation speed and feed rate of the forming tool on the thickness distribution and indicated that these parameters have no much influence on the thickness. Mirnia et al. [13] studied the effect of the tool diameter and the vertical pitch on the thickness distribution in SPIF of an aluminum alloy sheet using the finite element method (FEM) and experiments. It was stated that the minimum thickness does not monotonically increase with an increase of the vertical pitch and consequently an optimum vertical pitch can be found. The studies carried out by Mirnia et al. [14] on controlling the thinning and bottom bulging of the part during three-stage SPIF revealed that it is possible to reduce the thinning from 74% in the single-stage SPIF to 51% in the proposed three-stage strategy. Kurra et al. [15] focused on the optimization of the surface roughness in SPIF using genetic algorithm. They concluded that the optimum process parameters for an appropriate surface roughness are 10 mm, 0.15 mm, and 55° for the tool diameter, the vertical pitch, and the wall angle, respectively.

The applicability of SPIF is not limited to the sheet metal parts. Recently, the utilization of SPIF in the forming of thin-walled tubes has attracted much attention. Teramae et al. [16] conducted their studies on SPIF of branched tubes. The deformation strategy in SPIF of branched tubes was investigated by Yang et al. [17]. Sequences of the forming process using three and five-axis CNC machines with an improved bar tool were analyzed. Incremental forming of the tube end from 316 L stainless steel and AA6061 aluminum tubes was studied by Wen et al. [18] through the FEM simulation and experiments and two forming strategies were proposed. In the first strategy, the forming height in the intermediate stages is the same but the forming semi-angle increases gradually between successive stages. In the second strategy, the forming height increases gradually between successive stages while the forming semi-angle in the intermediate geometries is the same as the one in the final shape. As an industrial case study, Raujol-Veille et al. [19] implemented SPIF to manufacture an inner race of the low alloyed steel DC03 for a thrust bearing from an initial cylindrical ring and numerically investigated the forming process.

Regarding the advantages of SPIF over the conventional pressing process such as the higher formability and the low-cost tooling, implementing SPIF in the tube end forming can be a promising manufacturing process. Based on the literature reviewed above, limited works have dealt with this emerging forming process. The present research is focused on the further investigation of the incremental tube end flaring. In this way, experimental and numerical studies are carried out. The effects of different multistage strategies on the thickness distribution, the material deformation, and the formability are investigated, and a comparison with the conventional pressing is made. It is worth mentioning that due to the high flexibility of SPIF, the incremental tube end flaring is not restricted to the axisymmetric conical shapes and it is possible to form a wide

range of non-axisymmetric geometries. Therefore, the feasibility of the pyramidal flaring of the tube end using different multistage SPIF is analyzed to enhance the process window of the incremental tube end flaring.

2 Incremental tube end flaring

In the present paper, SPIF of the end of the aluminum tubes with the outer diameter of 40 mm and the initial thickness of 1 mm is considered. The considered geometry of the final expanded tube in the shape of a cone and a pyramid is depicted in Fig. 1. In this figure, α is the semi-apex angle of the truncated cone and pyramid. The corresponding length for flaring is 15 mm from the free end of the tube. In pyramidal flaring, the minor base of the truncated pyramid is assumed to be the average of the inscribed and circumscribed squares about the initial cross section of the tube. The chemical composition and the mechanical properties of the aluminum alloy are presented in Tables 1 and 2, respectively. The mechanical properties of the aluminum tube were captured using the uniaxial tension test according to ASTM E8-M along the axial direction. The Ludwik law was assumed to describe the work hardening behavior of the material as follows:

$$\sigma = \sigma_s + k\varepsilon^n \tag{1}$$

in which k and n are respectively the strength coefficient and the work hardening exponent as presented in Table 2.

The SPIF process was performed on a three-axis CNC milling machine as demonstrated in Fig. 2a. Figure 2b shows the designed rig for clamping the aluminum tube during SPIF. In Fig. 2b, the backing plate with a circular hole of the same diameter as the tube diameter is located on the upper plate firmly fixed by four supports on the lower plate. The aluminum tube is placed inside the designed rig from the top and held by means of a clamping system on the lower plate. The clamping system includes the movable and stationary parts. To ensure that the bottom end of the tube is firmly fixed and to avoid any rotation of the tube during the process, a polyurethane bar is located inside the tube and compressed by a screw to push the tube wall onto the clamping system. The experimental setup is mounted on the CNC machine as in Fig. 2. A hemispherical head tool with 10 mm diameter is utilized in incremental flaring along a predefined tool path with the feed rate of 1260 mm/min and no spindle rotation. According to Fig. 3a, b, the spiral and *Z*-constant tool paths with a desired vertical pitch are generated using the CAM software PowerMILL 13.0.06. Figure 3c, d illustrates the two kinds of tool movement considered in the present research along a predetermined tool path, namely top towards bottom (TB) movement and bottom towards top (BT) movement, respectively. Hydraulic oil is continuously fed in the forming region to reduce friction between the tool and the tube.

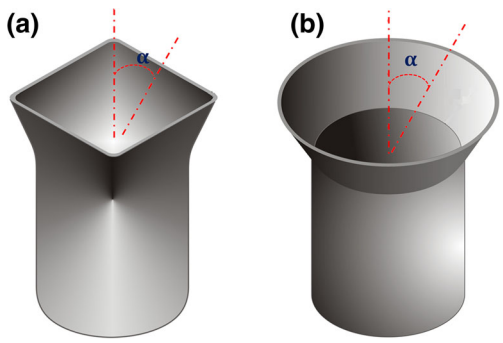

Fig. 1 Schematic illustration of flared tubes by SPIF in the shape of the truncated **a** pyramid and **b** cone

Table 1 The chemical composition of the aluminum alloy tube

Element	Fe	Si	Zn	Cu	Mg	Mn	Ti	Cr	Al
Weight %	1.6	0.54	0.33	0.28	0.17	0.10	0.02	0.01	Balance

As a comparison with SPIF of the tube end, a conventional pressing test for the same flaring process was experimentally conducted using a 25-ton hydraulic press depicted in Fig. 4a. In this way, a pressing die set was designed and made from cold working tool steel. Figure 4b shows the conical punches with the semi-apex angle of 10°, 15°, and 20°.

The thickness measurement was carried out using a vernier caliper with an accuracy of 0.01 mm along a desired cut section prepared by the wire EDM process and a surface roughness measurement device with a resolution of 0.001 μm was utilized to examine the surface quality. Circle grids with the diameter of 2.5 mm were electrochemically etched on the aluminum tube to measure major and minor in-plane strains, i.e., ε_1 and ε_2, experimentally. After the flaring process, in-plane principal strains were captured by measuring the major and minor diameters of the formed ellipses as follows:

$$\varepsilon_1 = \ln\left(\frac{d_1}{d_0}\right) \tag{2}$$

$$\varepsilon_2 = \ln\left(\frac{d_2}{d_0}\right) \tag{3}$$

in which d_0 is the initial circle diameter and d_1 and d_2 are the major and minor diameters of the deformed circle along

Table 2 The mechanical properties of the aluminum alloy tube

Properties	Symbol	Value
Density (kg/m^3)	ρ	2700
Young's modulus (GPa)	E	71
Poisson's ratio	ϑ	0.34
Yield stress (MPa)	σ_s	108.2
Strength coefficient (MPa)	k	318
Strain hardening exponent	n	0.34

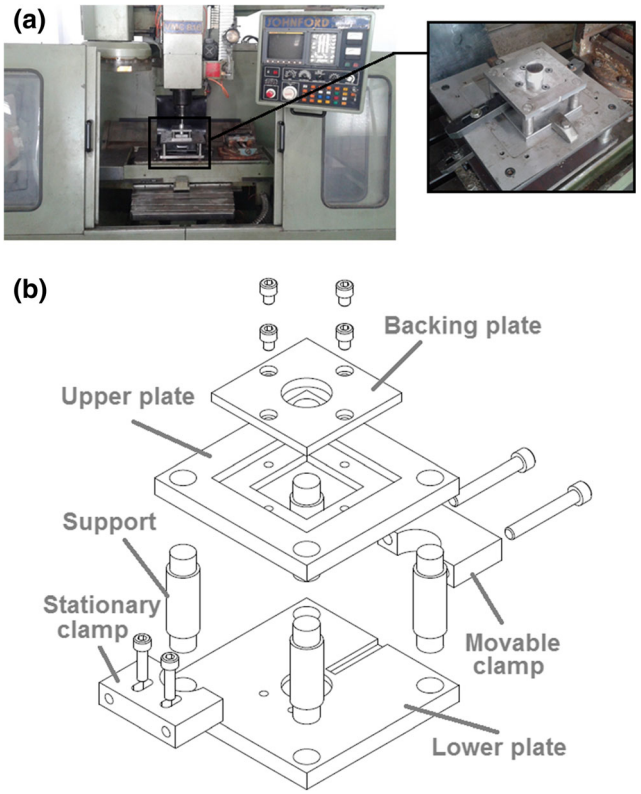

Fig. 2 **a** The experimental setup mounted on the CNC milling machine. **b** The exploded view of the designed rig for incremental tube end flaring

circumferential and axial directions, respectively, as demonstrated in Fig. 5.

In SPIF of metal sheets, the forming tool is initially tangent to the blank surface and its movement starts from the zero height along a predetermined path. But, the initial positioning of the forming tool in multistage SPIF of tube ends differs from the one in SPIF of metal sheets. According to Fig. 6a, in multistage SPIF of the tube end with an angular step of θ, the free end of the tube moves downwards gradually. Therefore, for the TB movement, the initial position of the forming tool in each stage should be calculated based on Fig. 6b. Otherwise, at the start of a stage, the forming tool approaches the tube from outside and pushes the free end such that a failure of the process can occur. Figure 7 depicts such a failure due to an improper position of the forming tool at the start of the second stage.

Regarding Fig. 6b, in *i*th stage of the forming process, the tool moves downwards in the Z direction along the path 1 and then traces the path 2 to arrive at the start point of the corresponding stage. In this instant, the tool is in contact with the tube edge (the point T corresponds to the contact position) which is pushed outwards. After that, the incremental flaring process is carried out along the predetermined tool path (spiral or Z-constant) up to the depth of L from the free end. If the tool movement starts from the bottom of the described path towards the top, the tool path is named the BT movement in which the end point of the path is the start point of the TB movement (Fig. 3c, d). The initial downward displacement of the tool along the Z direction (from o' to o) to reach the contact point T for *i*th stage can be calculated as follows:

$$Z_i = -(\Delta h_i + H_i) \tag{4}$$

in which Δh_i and H_i are obtained based on Fig. 6b as following:

$$\Delta h_i = L - L\cos\alpha \tag{5}$$

$$H_i = R \times (1 - \sin\alpha) \tag{6}$$

where L is the considered length of the tube in the flaring process, α is the semi-apex angle, and R is the forming tool radius. In Eqs. (4) and (5), Δh_i corresponds to the downward displacement of the free end in *i*th stage.

3 FE modeling of incremental tube end flaring

The FE modeling was carried out using the commercial code Abaqus/Explicit 6.13.3. To reduce CPU time, a time scaling scheme was utilized such that the ratio of the kinetic energy to the internal energy is less than 1% during the simulation. In this way, after a sensitivity analysis on the speed up factor, the velocity of the forming tool was artificially increased by a factor of 1050 as compared to the one in the experiment. To ensure that the tool path in the simulation is the same as the one in the experiment, the G-codes utilized in experiments were converted to appropriate inputs as the amplitudes defined in the boundary condition for the tool movement using a scripted code in the MATLAB environment.

The hemispherical head tool was modeled as an analytical rigid shell. The aluminum tube was discretized using 3075 shell elements S4R with five integration points through the thickness. Only the tube end, which is involved in the plastic deformation with the length of 25 mm from the free edge, was considered in the FE simulation as illustrated in Fig. 8. The plastic behavior of the tube was assumed isotropic and described using the Von Mises yield criterion. The elastic-plastic properties were defined as presented in Table 2. A fixed boundary condition was imposed at the bottom end of the tube to avoid any movements and rotations. The friction between the rigid tool and the tube was modeled using the Coulomb law with a coefficient of 0.05 according to [20].

4 Results and discussion

4.1 Validation of the FE model

The experiments of the incremental tube end flaring were conducted to validate the results of the FE simulation. In this

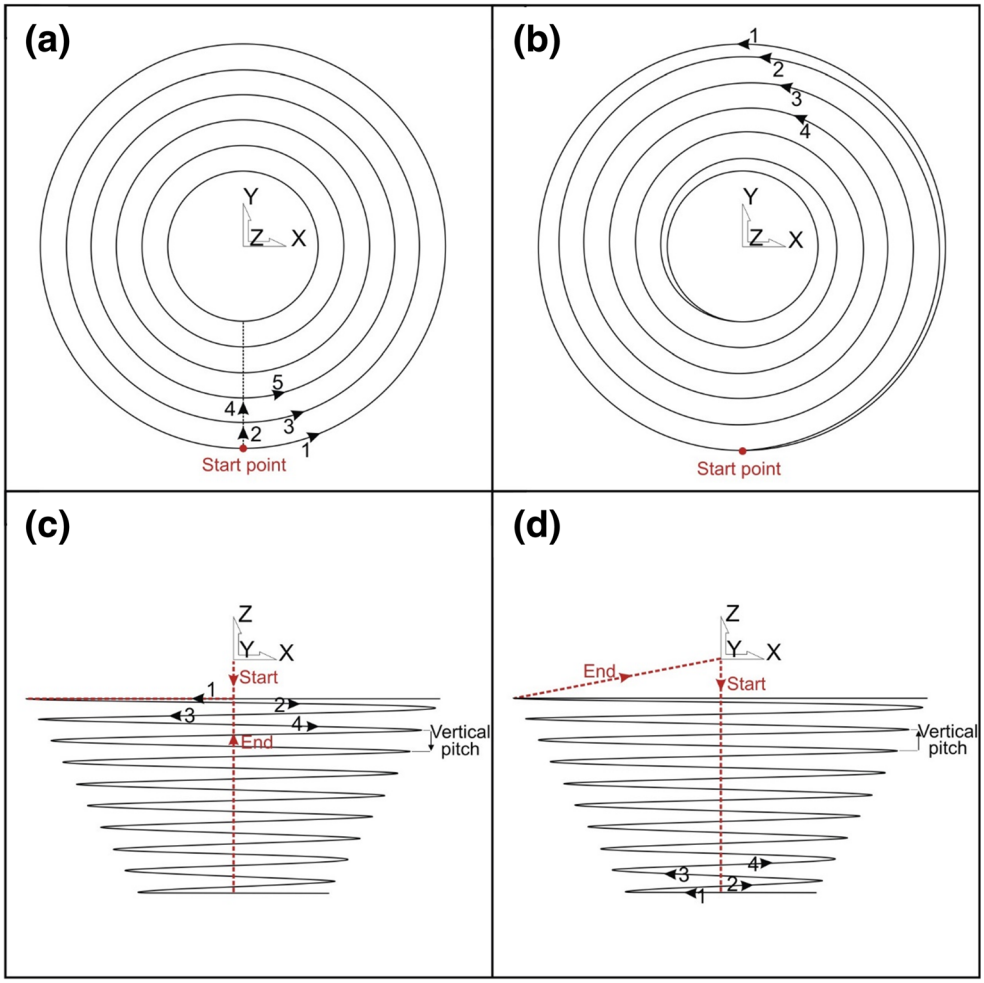

Fig. 3 The tool path and movement in incremental tube end flaring. **a** *Z*-constant path. **b** Spiral path. **c** Top towards bottom (TB) movement. **d** Bottom towards top (BT) movement

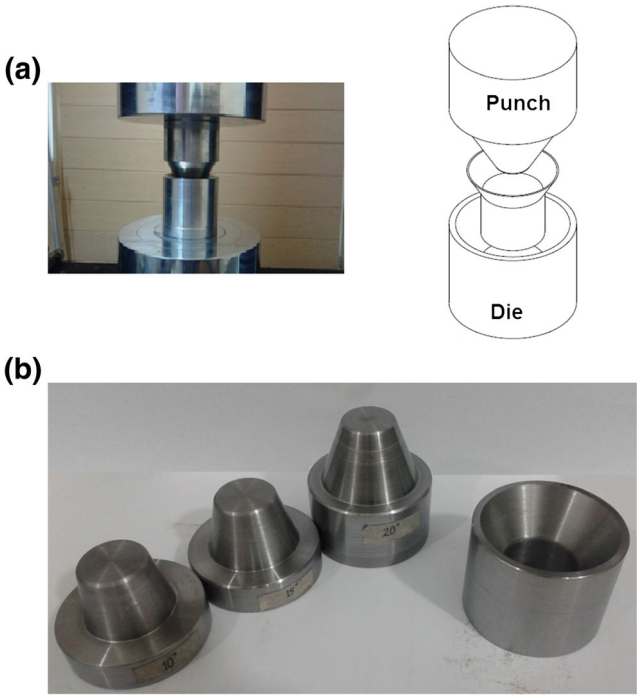

Fig. 4 **a** The conventional pressing die set. **b** The conical punches with different semi-angles and the utilized die

way, SPIF of the tube with a tool of 10 mm diameter along a spiral path was considered to expand the 15 mm length of the tube end in the shape of a truncated cone. The TB movement with an angular step of 5° was implemented. Figure 9 shows the thickness distribution for semi-cone angles of 10° and 25° along the longitudinal path illustrated on the simulated configuration. The true distance is the traveled length from the bottom of the longitudinal path towards the considered point. As seen, an appropriate agreement exists between experimental and numerical thickness distributions. The maximum deviation between the results of the FE simulation and

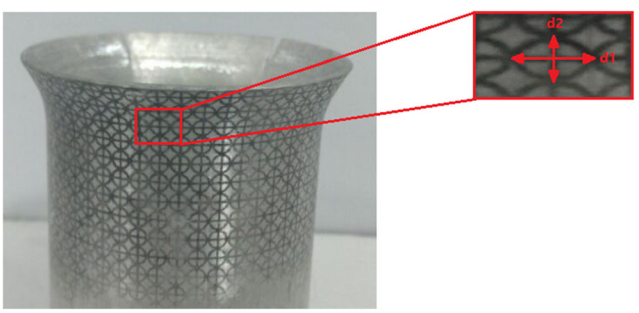

Fig. 5 Circle girds electrochemically etched on the aluminum tube

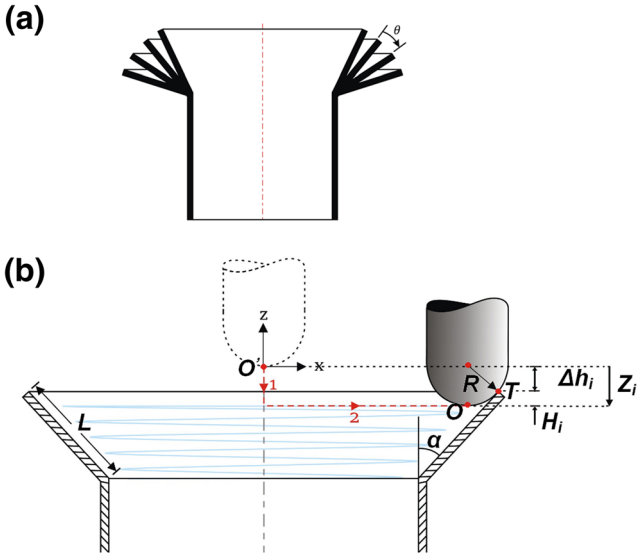

Fig. 6 **a** Multistage SPIF with an angular step of θ. **b** Calculation of the initial position of the forming tool for ith stage

experiment is less than 3% for the semi-angle of 10° (Fig. 9a) and 4% for the semi-angle of 25° (Fig. 9b). The major and minor in-plane strains obtained from the experiment and simulation on the outer surface of the tube are shown for the semi-cone angle of 55° at which the fracture occurred according to Fig. 10. It is obvious that the trend of in-plane strains can be reasonably captured by the FE model.

4.2 Forming strategies of incremental tube end flaring

The flaring process of the tube end using SPIF can be carried out through different forming strategies. In this section, the effect of different strategies on the material deformation is investigated. Regarding Fig. 3c, d, the forming tool can move along the predetermined path through either the TB or BT movement. In SPIF, the tube is subjected to concentrated loads asymmetrically while it is under uniformly distributed loads in pressing process. Accordingly, in order to avoid buckling and high forming forces, the incremental flaring process cannot be performed using a single-stage SPIF, and instead, a multistage strategy should be utilized. One of the possible multistage strategies is to increase the semi-apex angle gradually at

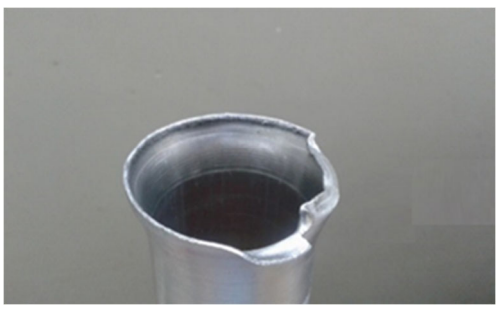

Fig. 7. A failure in incremental tube end flaring due to an improper positioning of the forming tool at the second stage

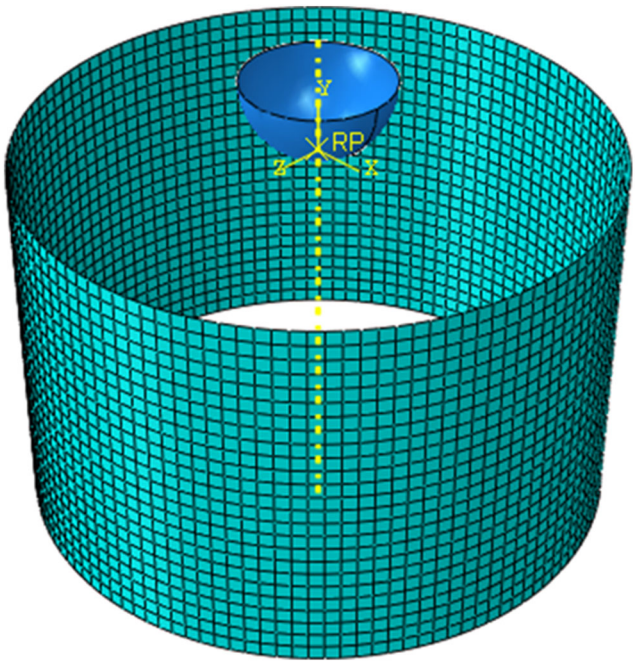

Fig. 8 The FE model of incremental tube end flaring

intermediate geometries with a specified angular step. Here, two angular steps of 5° and 10° are utilized for the TB movement. The BT movement is only considered with the angular

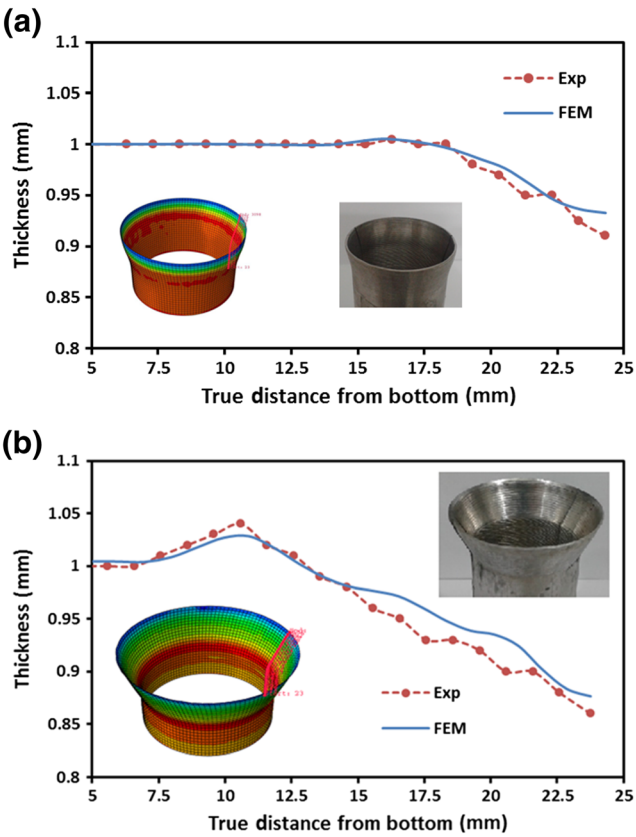

Fig. 9 Experimental and numerical thickness distributions at the semi-cone angles of **a** 10° and **b** 25°

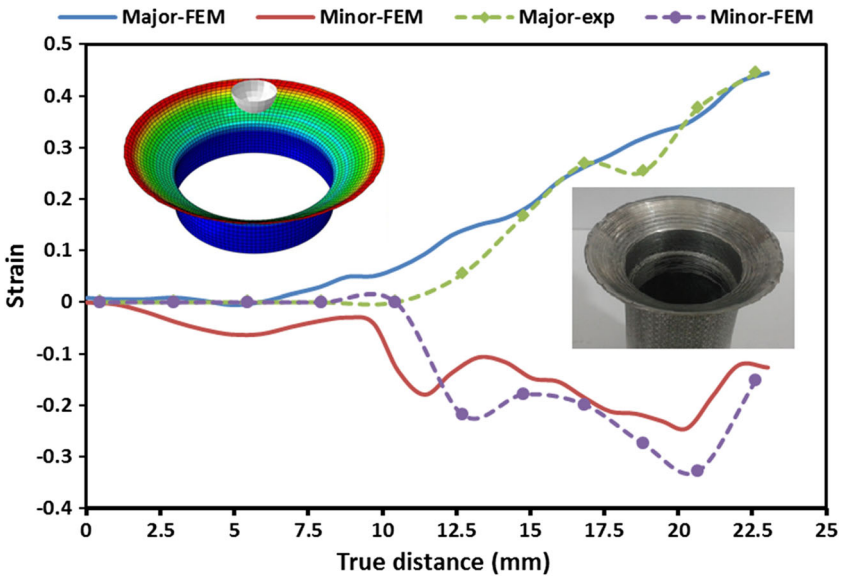

Fig. 10 In-plane strains on the outer surface of the tube at the semi-cone angle of 55° obtained from the experiment and FE simulation

step of 5°. The samples formed under the abovementioned strategies together with the maximum semi-apex angles before fracture are depicted in Fig. 11. For the sake of comparison, the maximum semi-angle achieved in pressing process has been also presented. Although it is possible to perform the pressing process in single-stage, the multistage strategy with the angular step of 5° was implemented such that the deformation condition remains the same for both the pressing and SPIF processes.

It is apparent from Fig. 11 that the highest possible semi-angle can be achieved using the TB movement with the angular step of 5°. As expected, regardless of the SPIF strategy, the maximum semi-angle achievable in incremental tube end flaring is higher than the one in pressing. Compared to pressing process ($\alpha_{\text{Pressing}} = 20°$), the maximum semi-angle is improved 175, 150, and 100% (as calculated by $\frac{\alpha_{SPIF} - \alpha_{Pressing}}{\alpha_{Pressing}} \times 100$) using the TB movement with the angular step of 5°, the TB movement with the angular step of 10°, and the BT movement with the angular step of 5°, respectively. Using the TB movement with fewer forming stages as a result of the larger angular step, the formability is reduced, but it is still higher than that in the BT movement.

Since in SPIF, the tube is deformed locally and incrementally and subjected to the successive bending and unbending, different mechanisms as mentioned by Emmens and van den Boogaard [21] can lead to the necking suppression and the formability enhancement compared to the conventional pressing process. For all samples of Fig. 11, the fracture was initiated

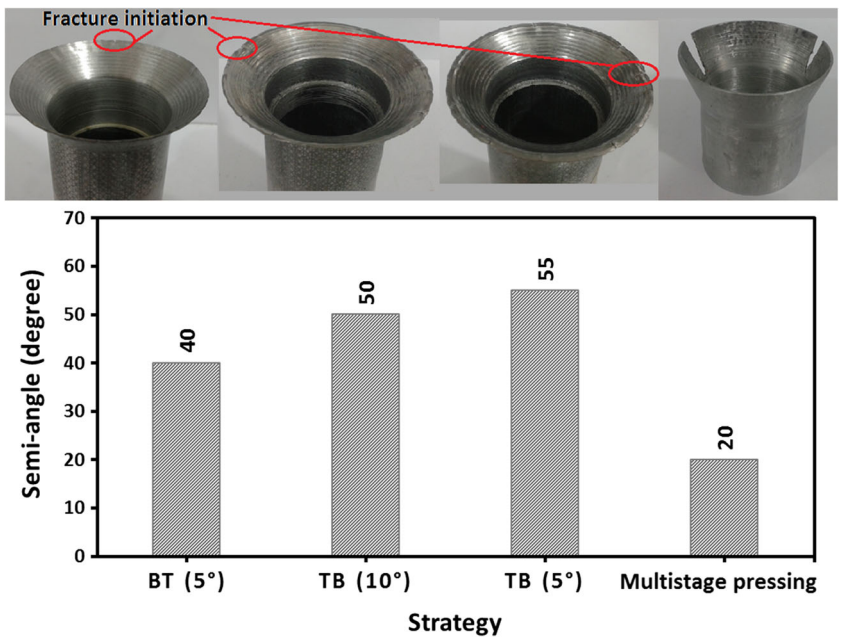

Fig. 11 The effect of different forming strategies on the maximum achievable semi-cone angle

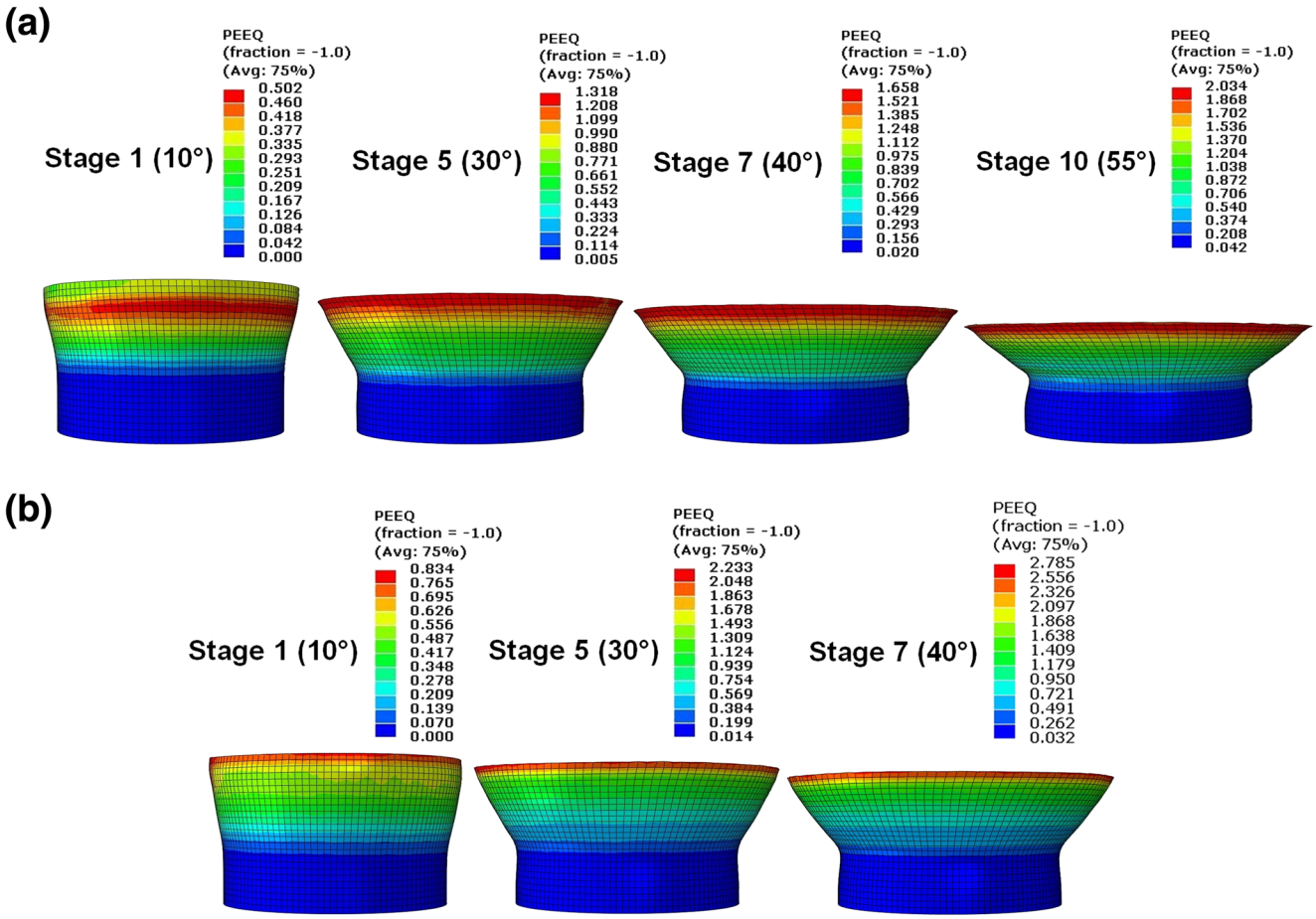

Fig. 12 Simulated configurations of intermediate stages for the **a** TB and **b** BT movements together with the equivalent plastic strain distributions

at the free edges. The FE simulations of abovementioned multistage strategies were carried out up to the last stage in the corresponding experiment in which the fracture occurred. Figure 12 indicates the simulated configurations together with the equivalent plastic strain distribution of the intermediate stages in the TB and BT movement with the angular step of 5°. By comparing the strain distribution in the same intermediate stages of both movements, it is apparent that the equivalent plastic strain in the BT movement is usually higher than that in the TB movement. The vertical displacement of the free end in the TB movement is higher than that in the BT movement at the same intermediate stage. The distribution of the equivalent plastic strain on the outer surface of the tube along the longitudinal direction is shown in Fig. 13 for the last stage of the considered multistage strategies. With respect to Figs. 12 and 13, owing to the more circumferential expansion, the free edges undergo larger equivalent plastic strain and so fracture is more likely to occur. The maximum equivalent plastic strain at

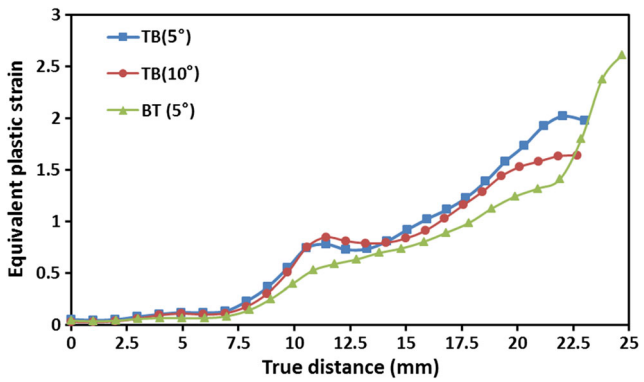

Fig. 13 The equivalent plastic strain distribution along the longitudinal path on the outer surface of the tube

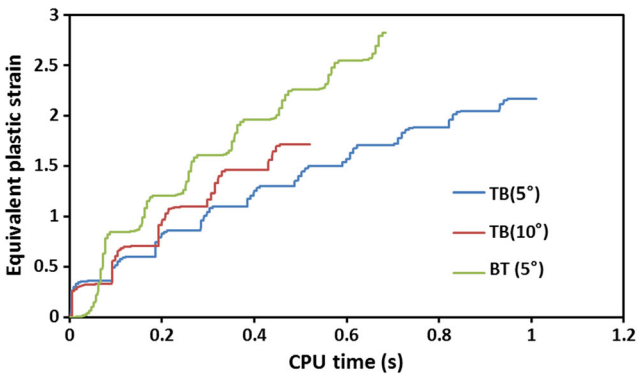

Fig. 14 The evolution of the equivalent plastic strain on the outer surface of an element with the highest value of the equivalent plastic strain

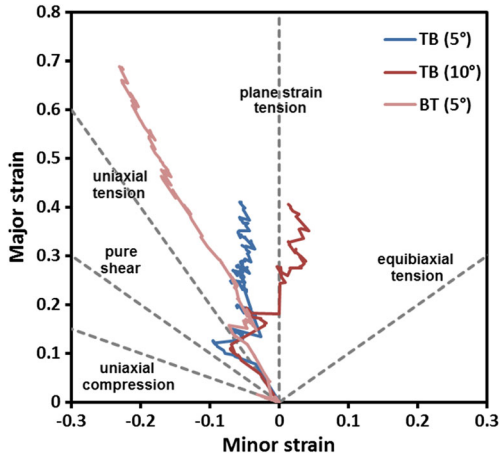

Fig. 15 The strain path of the element with the highest equivalent plastic strain in different forming strategies

the last stage in which the fracture occurs can be regarded as the fracture strain which is larger in the BT movement with fewer forming stages than the one in the TB movement. As depicted in Fig. 13, the equivalent plastic strain in the BT movement at each point far away from the free end is smaller than the one in the two other strategies because of the fact that the tube end undergoes less deformation in the BT movement with fewer stages. But, near the free edge, the equivalent plastic strain increases suddenly leading to a premature fracture.

With respect to ductile fracture mechanics, rupture is more likely to occur at the point with the highest equivalent plastic strain [22]. Figure 14 indicates the evolution of the equivalent plastic strain at the outer surface of an element located on the free edge of the tube for the three multistage incremental flaring strategies of Fig. 11. The strain evolution is stepwise that is the characteristic of multistage strategies in which each strain step corresponds to a forming stage. The equivalent plastic strain increases more gradually in the TB movement with the angular step of 5° than in the one with the angular step of 10°. This can lead to a premature fracture in the TB movement with the angular step of 10°. At the angular step of 5°, the equivalent plastic strain increases more rapidly in the BT movement than in the TB movement. Small steps can be observed in Fig. 14 for each increase in the equivalent plastic strain at the respective stage. Such small steps can be related to the successive deformation of an element in SPIF at a particular forming stage.

The strain path of the element with the highest value of the equivalent plastic strain, located on the free edge of the tube, is demonstrated in the space of the in-plane principal strains of Fig. 15 for the multistage SPIF strategies. As seen, the strain path is non-linear which can be attributed to the localized and incremental nature of deformation in multistage SPIF. The fracture limit of the material can be significantly affected by the non-proportional loading path [23]. The highly non-linear strain path suggests the existence of redundant strains due to successive bending and unbending during SPIF. These redundant strains induced differently during the investigated forming strategies can affect the distribution and accumulation of the equivalent plastic strain, as shown in Figs. 12, 13, and 14). Varying the forming strategy, the strain path goes from the strain state close to the uniaxial tension towards the plane strain tension. From the deformed circle grids shown in Fig. 11, it is apparent that the in-plane major in-plane strain is along the circumferential direction and the minor in-plane strain is along the axial direction. The final state of the in-plane principal strains at the outer surface of all elements is depicted in Fig. 16. So, Fig. 16 demonstrates the effect of the forming strategy on the strain state. The strain states near the origin of the diagram correspond to the bottom region of the tube and the ones far away from the origin correspond to the free edge. The strain states in the TB movement with the angular steps of 5° and 10° are the same except at the regions far away from the free edge, in which strain states for the angular step of 10° tend to be plane strain. In the BT movement, the majority part of the tube experiences the plane strain

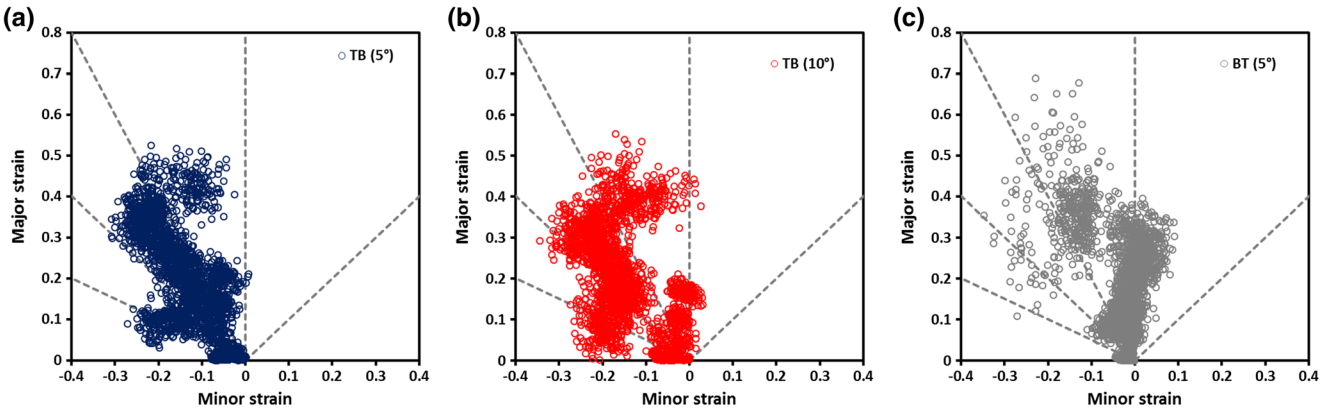

Fig. 16 The state of in-plane principal strains on the outer surface of the tube at the end of forming process. **a** The TB movement with 5° angular step. **b** The TB movement with 10° angular step. **c** The BT movement with 5° angular step

state, but the free edges undergo the strain state close to the uniaxial tension. Regions under the uniaxial compression, which can potentially lead to wrinkling, are much more in the TB movement rather than in the BT movement.

Figure 17 shows the thickness distribution of the aluminum tube in each forming stage of the TB movement with the 5° angular step up to the semi-cone angle of 30° along the longitudinal direction in which the true distance is calculated from the fixed end. In Fig. 17, two different regions on the tube wall can be distinguished, namely thickening and thinning regions. Since the tube undergoes the circumferential expansion in the flaring process, the thinning region appears on the wall such that the minimum thickness occurs at the free edge with the highest expansion. By increasing the semi-cone angle at each forming stage, the thinning gradually increases. As the forming process proceeds, the thickening also becomes larger. The observed thickening region can be attributed to the axial compressive stress imposed on the bottom of the deformation field during the process.

The thickness distribution obtained from the FE simulation in the incrementally flared tube up to the semi-cone angle of 30° using the considered multistage strategies is shown in Fig. 18. On the tube wall, the thinning is higher in the BT movement than in the TB movement, but on the free edge, the thinning is the same for both movements. An approximately identical trend of the thickness variation exists in the TB movement with different angular steps. In the TB movement, the tube wall is thicker using the angular step of 10° instead of

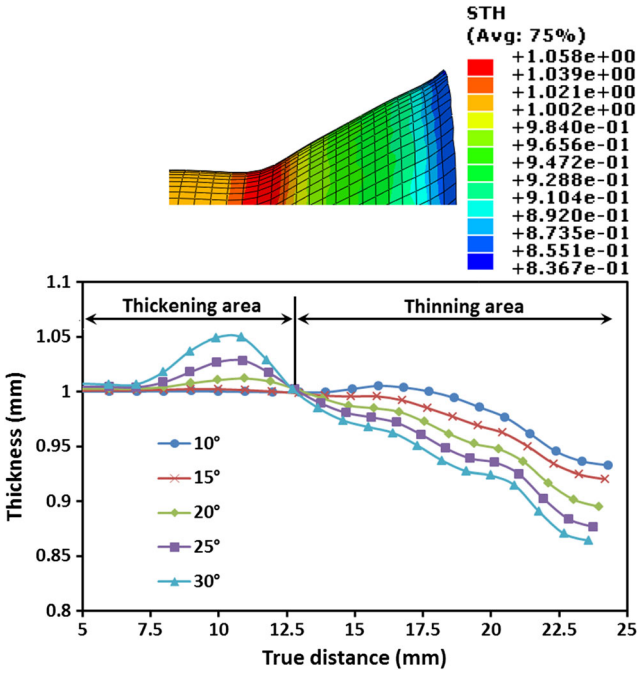

Fig. 17 The thickness distribution in each SPIF stage of the TB movement with the angular step of 5° up to the semi-cone angle of 30° predicted using the FE simulation

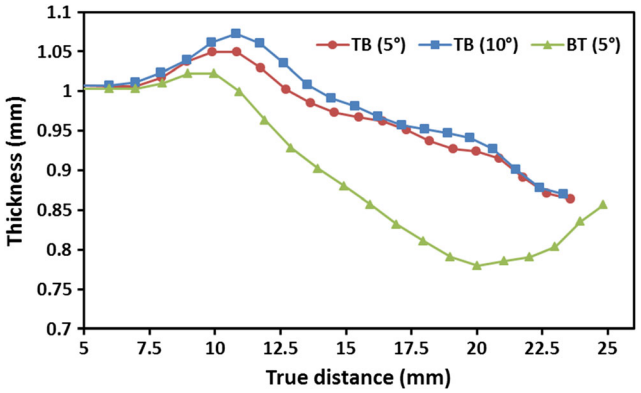

Fig. 18 The thickness distribution obtained from the FE simulation for different multistage strategies at the semi-cone angle of 30°

5°, but at the free edge, the equal thickness is observed. As in the BT movement, the material undergoes the plastic deformation from bottom towards the top, the axial compressive stress is reduced, and consequently it can be seen from Fig. 18 that the thickening becomes smaller.

The type of tool path can be regarded as a subcategory of the SPIF strategy. For further investigation, the spiral and *Z*-constant tool paths with the vertical pitch of 1 mm were considered in the TB movement with the angular step of 5°. Figure 19 compares the thickness distributions obtained from the numerical model at the semi-cone angle of 30° for the both tool paths. According to Fig. 19, by utilizing the spiral tool path rather than the *Z*-constant tool path, the maximum thinning and thickening can be reduced by 5 and 2%, respectively. In the spiral tool path, the material undergoes a smoother and more uniform plastic deformation than in the *Z*-constant tool path in which the forming tool descends by the amount of the vertical pitch suddenly at the end of each circular contour path.

The effect of the vertical pitch on the thickness distribution was numerically investigated and depicted in Fig. 20. The incremental tube end flaring was performed up to the semi-

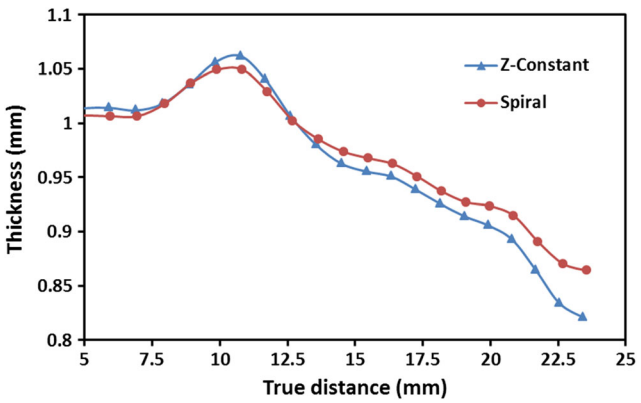

Fig. 19 The thickness distribution obtained from the FE simulation using the TB movement with the angular step of 5° through the spiral and *Z*-constant tool path at the semi-cone angle of 30°

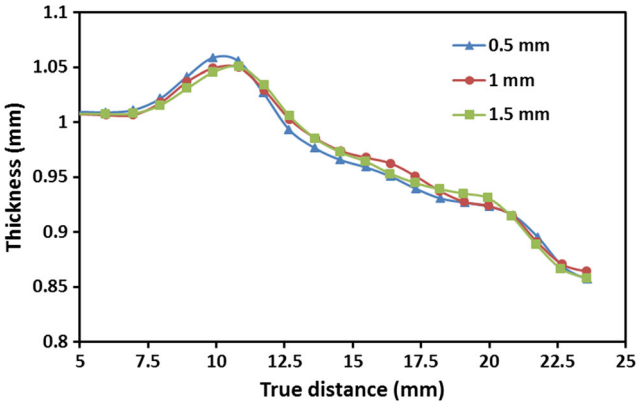

Fig. 20 The thickness distribution obtained from the FE simulation using the TB movement with the angular step of 5° and the spiral tool path for different values of the vertical pitch

cone angle of 30° using the spiral tool path and the TB movement with the angular step of 5°. As can be seen, the vertical pitch in the considered range of the present research has no significant effect on the thickness distribution. The possible reason may be attributed to the small angular step between two successive stages. As discussed in detail by Mirnia et al. [13] for the single-stage SPIF of a truncated cone, the vertical pitch can affect the thickness distribution through its effect on the bending and stretching deformation modes. But here, a multistage SPIF with a small angular step is considered and consequently bending and stretching effects of the vertical pitch on the thickness distribution diminish. Besides the thickness distribution, the surface roughness of the flared tube is strongly dependent on the vertical pitch, as depicted in Fig. 21. As expected, by increasing the vertical pitch, the surface roughness increases.

4.3 Pyramidal flaring of the tube end using multistage SPIF

One of the most prominent advantages of SPIF is its high flexibility to form symmetric and asymmetric parts. In this section, SPIF of the tube end in the shape of a truncated pyramid with the semi-apex angle of 20° is considered. To this end, different three-stage forming strategies are implemented. At the first forming strategy (named as strategy #1), the semi-apex angle increases gradually in each stage and the intermediate geometries are pyramids with the semi-apex angles of 10° and 15°. Since the initial cross section of the tube is circular, at the first stage, the corners undergo more deformation and the pyramid wall is formed at the following stages. Hence, the second strategy (named as strategy #2) was designed such that a truncated cone with the semi-apex angle of 10° and a truncated pyramid with the semi-apex angle of 15° are formed at the first and second stages, respectively. At the third strategy (named as strategy #3), intermediate geometries include the truncated cones with the semi-apex angles of 10° and 15°. For the described multistage strategies, the TB movement with a spiral tool path and the vertical pitch of 1 mm was utilized. Simulated configurations at each stage of the abovementioned strategies are demonstrated in Fig. 22. As can be seen, the free edge at last stages has some slight variations in the formed height resembling the so-called earing phenomenon. The slight earing observed at the free edge can be attributed to the more deformation imposed on the corners and the less deformation of the wall. From Fig. 22, it can be observed that the equivalent plastic strain in the last stages is highest at the corners. Since for strategy #1 the forming tool moves along a square path at the first stage, only the corners of the tube are formed. Consequently, in

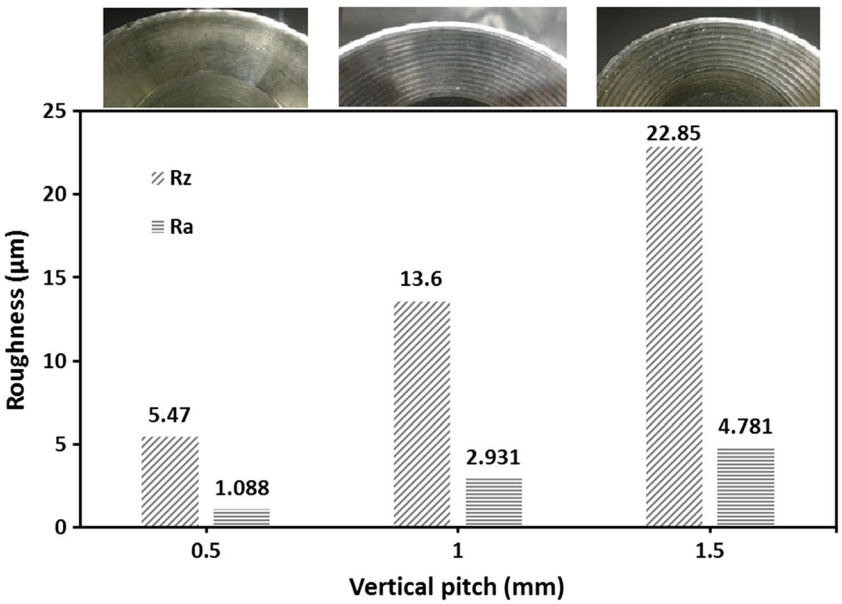

Fig. 21 Surface roughness at different values of the vertical pitch using the TB movement with the angular step of 5° and the spiral tool path

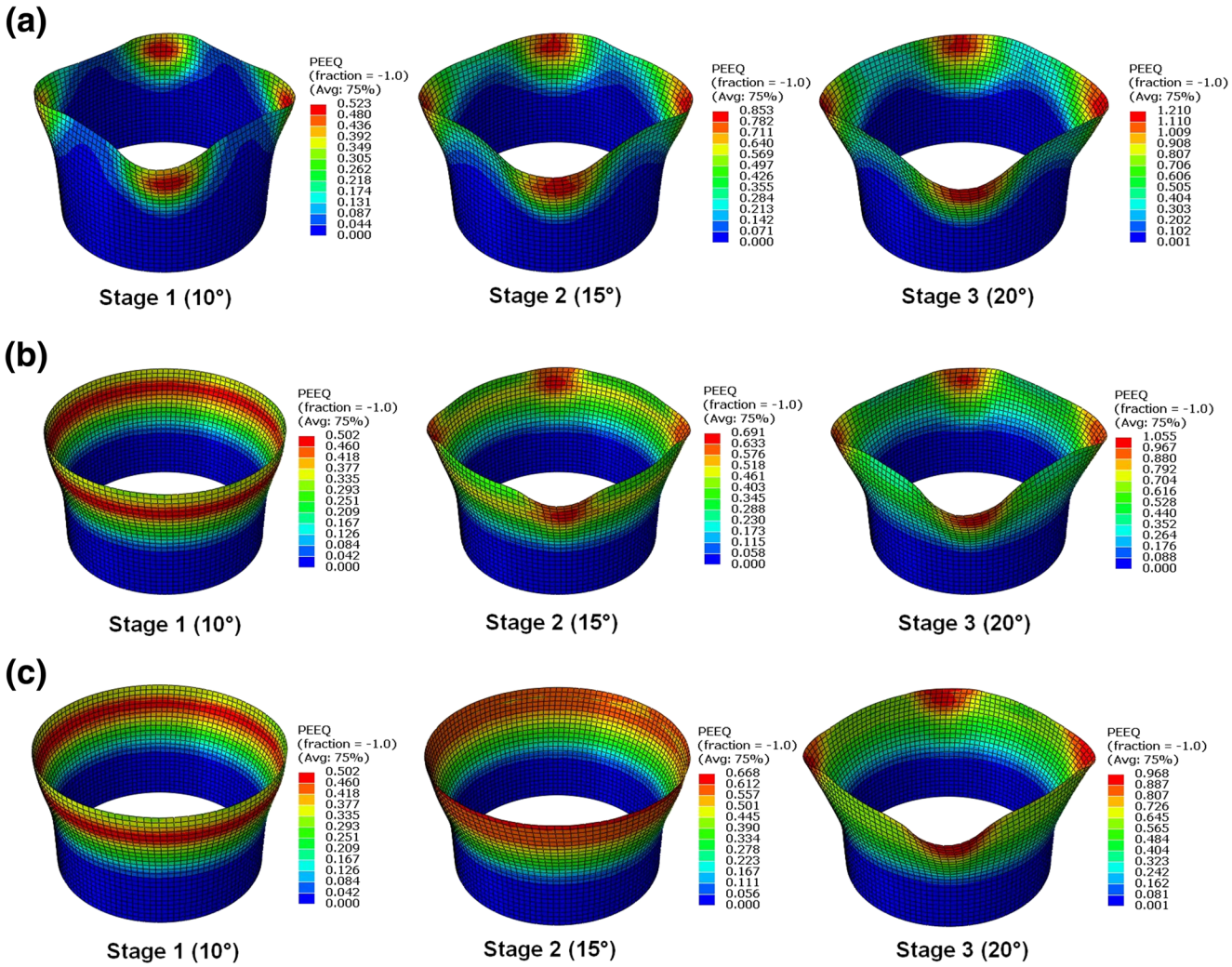

Fig. 22 Simulated configurations using the FE model in intermediate forming stages. **a** Strategy #1. **b** Strategy #2. **c)** Strategy #3

strategy #1 at the first stage, the tube wall undergoes a less plastic deformation, and in contrast, the corners have the largest equivalent plastic strain. In the other two strategies, because of forming a truncated cone at the first stage, the wall is also subjected to the large plastic deformation. As a result in the strategy #1 at the third strategy, the equivalent strain of the corners is higher than the one in the other two strategies and the less deformation occurs in the wall. Similarly, the corners of

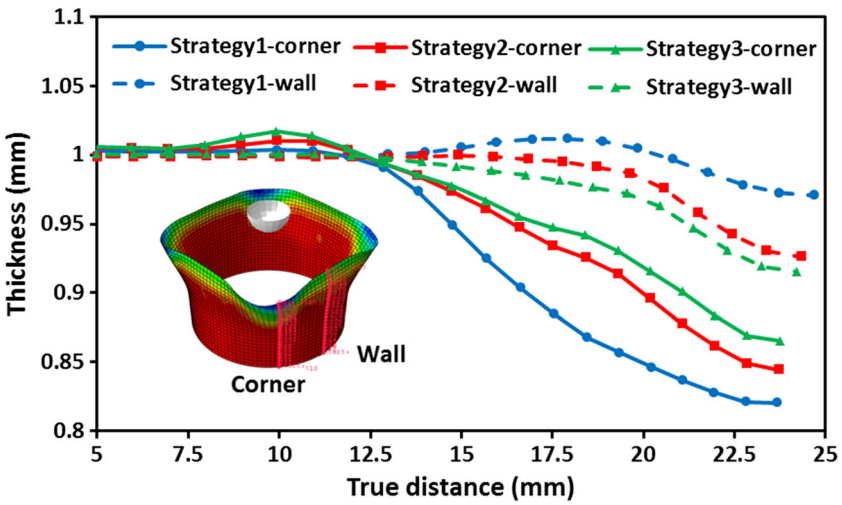

Fig. 23 Predicted thickness distributions for different three-stage forming strategies

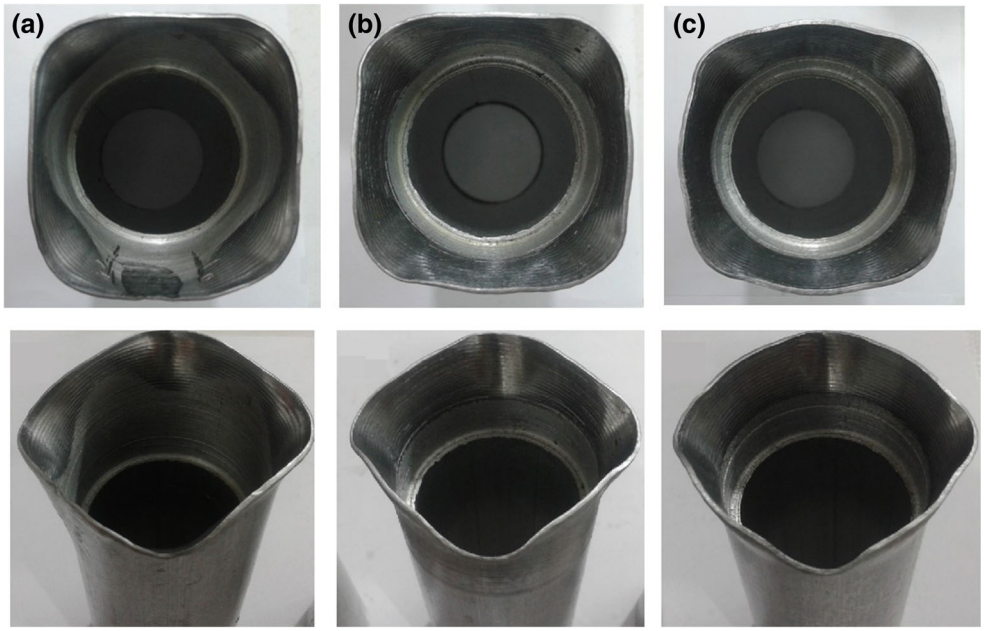

Fig. 24 Flared tubes in the shape of a truncated pyramid using multistage SPIF. **a** Strategy #1. **b** Strategy #2. **c** Strategy #3

the flared tube at the last stage in strategy #2 exhibit a larger equivalent strain than that in strategy #3.

The predicted thickness distribution at the wall and corners of the flared tube in the three multistage strategies is shown in Fig. 23. Regarding the above explanations, it can be seen that the material thinning at the wall and the corners of the aluminum tube flared using strategy #1 is respectively lower and higher than the one formed through the other two strategies and consequently, strategy #1 leads to a more non-uniform thickness distribution. As thinning of the wall and corners of the formed tube gets closer together in strategy #3, a more uniform thickness distribution is achieved. This is due to the fact that the intermediate geometries in strategy #3 are truncated cones by which the tube wall is much more involved in the deformation process. On the other hand, it is qualitatively clear that the flared tube using strategy #1 has a closer cross section to the expected square profile of the truncated pyramid than the one obtained by strategy #3, according to Fig. 24. In strategy #3, the forming tool moves along the square path only at the last stage and so, the wall of the truncated pyramid cannot be properly formed. Accordingly, by varying the multistage strategy from strategy #1 to strategy #3, the thickness distribution becomes more uniform and, conversely, the dimensional accuracy gets worse.

5 Conclusions

In the present research, multistage SPIF was utilized in the end flaring process of thin-walled aluminum tubes. The conical and pyramidal flaring processes of the tube end were considered. Through experiments and FE modeling using the commercial code Abaqus/Explicit, the effect of various designed forming strategies on the thickness distribution, the material deformation, and the tube formability was investigated. The comparison of the thickness distribution and the in-plane principal strains shows an appropriate agreement between the FE modeling and the experiment. Accordingly, the following conclusions can be drawn:

- Compared to the pressing process for conical flaring of the tube end, the maximum achievable semi-apex angle can be improved by 175, 150, and 100% using the TB movement with the angular step of 5°, the TB movement with the angular step of 10°, and the BT movement with the angular step of 5°, respectively.
- The thickness distribution and the strain state are significantly influenced by the forming strategy of the multistage process affecting the tube formability. It can be found from the results that using the BT movement, the tube thickening is more reduced compared to the TB movement.
- At the considered range for the forming parameters, the vertical pitch has a negligible effect on the thickness distribution of the incrementally flared tube. On the other hand, the surface roughness is highly dependent on the vertical pitch such that with increasing the vertical pitch, the surface roughness increases.
- Non-axisymmetric flaring of the tube end using the multistage SPIF is possible. By means of the designed three-stage strategies, it was shown that the thickness distribution is improved using the intermediate geometries in the form of the truncated cones with the semi-apex angles lower than the semi-angle of the final part, but the dimensional accuracy becomes worse. On the other hand, using

the truncated pyramids with lower semi-apex angles as the intermediate parts can result in an enhanced dimensional accuracy.

As future work, the dimensional accuracy in incremental tube end flaring which needs further investigation and improvement will be studied. Here, the effect of the deformation strategy was mainly investigated, as well as the effect of the tool path and the vertical pitch. In the future, effects of the other key parameters which have not been considered here, including the forming tool diameter, the feed rate, the spindle speed, and the lubrication, will be studied on the process performance.

Compliance with ethical standards

Conflict of interest The authors declare that they have no conflict of interest.

References

1. Huang Y-M (2004) Finite element analysis of tube flaring process with a conical tool. Int J Adv Manuf Technol 24(1):91–97. https://doi.org/10.1007/s00170-003-1704-0
2. Lu Y-H (2004) Study of tube flaring ratio and strain rate in the tube flaring process. Finite Elem Anal Des 40(3):305–318. https://doi.org/10.1016/S0168-874X(03)00049-0
3. Almeida BPP, Alves ML, Rosa PAR, Brito AG, Martins PAF (2006) Expansion and reduction of thin-walled tubes using a die: experimental and theoretical investigation. Int J Mach Tools Manuf 46(12–13):1643–1652. https://doi.org/10.1016/j.ijmachtools.2005.08.018
4. Huang YM (2009) Flaring and nosing process for composite annoy tube in circular cone tool application. Int J Adv Manuf Technol 43(11):1167–1176. https://doi.org/10.1007/s00170-008-1795-8
5. Nikhare CP, Korkolis YP, Kinsey BL (2015) Formability enhancement in titanium tube-flaring by manipulating the deformation path. J Manuf Sci Eng 137(5):051006–051006. https://doi.org/10.1115/1.4030512
6. Zhao X, Xu W, Chen Y, Ma H, Shan D, Lin H (2016) Fabrication of curved generatrix workpiece of TA15 titanium alloy by variable thickness tube spinning and flaring process. Int J Adv Manuf Technol 88:1–10. https://doi.org/10.1007/s00170-016-8917-5
7. Jackson KP, Allwood JM, Landert M (2008) Incremental forming of sandwich panels. J Mater Process Technol 204(1–3):290–303. https://doi.org/10.1016/j.jmatprotec.2007.11.117
8. Shim M-S, Park J-J (2001) The formability of aluminum sheet in incremental forming. J Mater Process Technol 113(1–3):654–658. https://doi.org/10.1016/S0924-0136(01)00679-3
9. Hussain G, Gao L (2007) A novel method to test the thinning limits of sheet metals in negative incremental forming. Int J Mach Tools Manuf 47(3–4):419–435. https://doi.org/10.1016/j.ijmachtools.2006.06.015
10. Jackson K, Allwood J (2009) The mechanics of incremental sheet forming. J Mater Process Technol 209(3):1158–1174. https://doi.org/10.1016/j.jmatprotec.2008.03.025
11. Manco GL, Ambrogio G (2010) Influence of thickness on formability in 6082-T6. Int J Mater Form 3(1):983–986. https://doi.org/10.1007/s12289-010-0934-6
12. Hamilton K, Jeswiet J (2010) Single point incremental forming at high feed rates and rotational speeds: surface and structural consequences. CIRP Ann Manuf Technol 59(1):311–314. https://doi.org/10.1016/j.cirp.2010.03.016
13. Mirnia MJ, Mollaei Dariani B, Vanhove H, Duflou JR (2014) An investigation into thickness distribution in single point incremental forming using sequential limit analysis. Int J Mater Form 7(4):469–477. https://doi.org/10.1007/s12289-013-1143-x
14. Mirnia MJ, Mollaei Dariani B, Vanhove H, Duflou JR (2014) Thickness improvement in single point incremental forming deduced by sequential limit analysis. Int J Adv Manuf Technol 70(9):2029–2041. https://doi.org/10.1007/s00170-013-5447-2
15. Kurra S, Hifzur Rahman N, Regalla SP, Gupta AK (2015) Modeling and optimization of surface roughness in single point incremental forming process. J Mater Res Technol 4(3):304–313. https://doi.org/10.1016/j.jmrt.2015.01.003
16. Teramae T, Manabe K, Ueno K, Nakamura K, Takeda H (2007) Effect of material properties on deformation behavior in incremental tube-burring process using a bar tool. J Mater Process Technol 191(1–3):24–29. https://doi.org/10.1016/j.jmatprotec.2007.03.039
17. Yang C, Wen T, Liu LT, Zhang S, Wang H (2014) Dieless incremental hole-flanging of thin-walled tube for producing branched tubing. J Mater Process Technol 214(11):2461–2467. https://doi.org/10.1016/j.jmatprotec.2014.05.027
18. Wen T, Yang C, Zhang S, Liu L (2015) Characterization of deformation behavior of thin-walled tubes during incremental forming: a study with selected examples. Int J Adv Manuf Technol 78(9):1769–1780. https://doi.org/10.1007/s00170-014-6777-4
19. Raujol-Veillé J, Toussaint F, Tabourot L, Vautrot M, Balland P (2015) Experimental and numerical investigation of a short, thin-walled steel tube incremental forming process. J Manuf Process 19:59–66. https://doi.org/10.1016/j.jmapro.2015.03.008
20. Zhang MH, Lu B, Chen J, Long H, Ou H (2015) Selective element fission approach for fast FEM simulation of incremental sheet forming based on dual-mesh system. Int J Adv Manuf Technol 78(5):1147–1160. https://doi.org/10.1007/s00170-014-6723-5
21. Emmens WC, van den Boogaard AH (2009) An overview of stabilizing deformation mechanisms in incremental sheet forming. J Mater Process Technol 209(8):3688–3695. doi:https://doi.org/10.1016/j.jmatprotec.2008.10.003
22. Mirnia MJ, Shamsari M (2017) Numerical prediction of failure in single point incremental forming using a phenomenological ductile fracture criterion. J Mater Process Technol 244:17–43. https://doi.org/10.1016/j.jmatprotec.2017.01.029
23. Benzerga AA, Surovik D, Keralavarma SM (2012) On the path-dependence of the fracture locus in ductile materials—analysis. Int J Plast 37:157–170. doi:https://doi.org/10.1016/j.ijplas.2012.05.003